Phase transitions in models for coupled charge-density waves

Minchul Lee,[1] Eun-Ah Kim,[2] Jong Soo Lim,[3] and M. Y. Choi,[3,4]
[1]*Department of Physics, Korea University, Seoul 136-701, Korea*
[2]*Department of Physics, University of Illinois, Champaign, Illinois 61801, USA*
[3]*Department of Physics, Seoul National University, Seoul 151-747, Korea*
[4]*Korea Institute for Advanced Study, Seoul 130-722, Korea*
(Received 16 October 2003; published 22 March 2004)

Various phase transitions in models for coupled charge-density waves are investigated by means of the ϵ expansion, mean-field theory, and Monte Carlo simulations. At zero temperature the effective action for the system with appropriate commensurability effects is mapped onto the three- or four-dimensional XY model, depending on spatiotemporal fluctuations, under the corresponding symmetry-breaking fields. It is revealed that the three- and four-dimensional systems display a single transition between the clock order (with broken Z_M symmetry) and disorder. The nature of the phase transition depends crucially on the commensurability factor M: For $M \geqslant 4$, in particular, the transition belongs to the same university class as the XY model. On the other hand, in the presence of misfit causing frustration in the charge-density wave, the interchain coupling is observed to favor either the commensurate state or the incommensurate state depending on the initial configuration; this gives rise to hysteresis around the commensurate-incommensurate transition. Boundaries separating such phases with different symmetries are obtained in the parameter space consisting of the temperature, symmetry-breaking field, fluctuation strength, interchain coupling, and misfit.

DOI: 10.1103/PhysRevB.69.115117 PACS number(s): 71.45.Lr, 64.60.Cn, 64.70.Rh

I. INTRODUCTION

A large number of organic and inorganic solids have crystalline structures in which fundamental structural units form linear chains.[1] In these materials, largely different overlaps of the electronic wave functions in various crystallographic directions lead to strongly anisotropic, so-called quasi-one-dimensional (quasi-1D) electron bands. Among the exotic physical phenomena in quasi-1D materials, charge-density waves (CDW's) are of much continual interest. Research into this topic has been stimulated by recent advances in experimental techniques, which now allow direct observation of CDW's and measurement of various static and dynamic properties of CDW systems.[2] In general the material of quasi-1D structure is expected to exist in the form of a bundle of chains rather than of a single chain. In such a bundle of chains, interchain tunneling of electrons leads to coupling of the fluctuations on neighboring chains, which may affect the behavior of the system in a crucial way. For example, the system of two coupled incommensurate chains in the weak-coupling limit has been reported to exhibit a complicated commensurate-incommensurate (CI) transition, reminiscent of devil's staircase.[3] Obviously, the opening of the gap at the Fermi surface implies that each separate chain is an insulator at low temperatures. However, with the coupling between chains taken into account, expected are various transitions between insulating and metallic phases, the extensive investigation of which is still lacking in spite of the ubiquity of the CDW.

In this paper, we investigate nature of the phase transitions in the coupled CDW system. In the absence of misfit the effective action for the (commensurate) system at zero temperature with suitable commensurability effects is mapped onto the XY model under the corresponding symmetry-breaking field. The effective dimension of the system is given by four if both spatial and temporal fluctuations are significant, otherwise it is three. The phase transition in the resulting 3D XY model under the appropriate symmetry-breaking field is examined via the ϵ expansion and the Monte Carlo method. It is found that there emerges in the system the clock ordered phase (with the Z_M symmetry broken) via a second-order transition, the nature of which depends on the commensurability factor M: In particular, the critical behavior for $M \geqslant 4$ appears to be the same as that of the 3D XY model. For the 4D XY model, on the other hand, mean-field theory is expected to be accurate and reveals a single transition, which is of the first order for $M=3$ and of the second order otherwise. We then examine the effects of misfit, which not only change the nature of the order-disorder transition but also brings about a CI transition. In the presence of the misfit, correlations due to the interchain coupling are observed to favor, depending on the initial configuration, either the commensurate state or an incommensurate state, which gives rise to hysteresis behavior: While in the cooling process the incommensurate CDW's persist near zero temperature, in the heating process large portions of the system remain in the commensurate state at rather high temperatures.

This paper is organized as follows. In Sec. II, the effective action at zero temperature is derived for the coupled CDW system and mapped onto the appropriate XY model according to whether spatial and/or temporal fluctuations are taken into consideration. Section III is devoted to the investigation of the phase transition in the 3D XY model under the symmetry-breaking field, which introduces the Z_M symmetry to the system. Here two independent approaches are employed: the ϵ expansion in Sec. III A and the Monte Carlo method in Sec. III B. Section IV presents the mean-field analysis of the 4D XY model, demonstrating the first- and second-order nature of the transition under the appropriate

symmetry-breaking field. In Sec. V the effects of the interchain coupling in the presence of misfit are investigated via Monte Carlo simulations, which discloses properties of the CI transition in the system. Combining the results for the CI transition with those for the 3D and 4D XY models obtained in Secs. III and IV, we construct in Sec. VI schematic phase diagrams for general coupled CDW systems in the 3D space consisting of the temperature, interchain coupling, and misfit. Finally, Sec. VII gives a brief summary.

II. EFFECTIVE ACTION

We consider a system of coupled near-commensurate CDW chains along the z direction, each of which is characterized by the commensurability factor M and the position-dependent misfit $\delta_{\mathbf{r}}$ with $\mathbf{r}=(x,y,z)$. On the x-y plane, the chains are assumed for simplicity to constitute a square array of lattice constant $a\,(\equiv 1)$. Disregarding amplitude fluctuations of the complex CDW order parameter and considering spatial and temporal fluctuations of the phase only,[4] we write the Hamiltonian in terms of the phase $\phi_{\mathbf{r}}$ of the order parameter at position $\mathbf{r}$ and the momentum $p_{\mathbf{r}}=C\partial\phi_{\mathbf{r}}/\partial t$:

$$\mathcal{H}_1=\int dz\sum_{x,y}\left[\frac{p_{\mathbf{r}}^2}{2C}+\frac{U_\parallel}{2}\left(\frac{\partial\phi_{\mathbf{r}}}{\partial z}-\delta_{\mathbf{r}}\right)^2-V_0\cos M\phi_{\mathbf{r}}\right], \tag{1}$$

where for the moment the interchain coupling has been omitted. The first term and the second term correspond to the change of the total electron kinetic energy due to temporal and spatial fluctuations, respectively, whereas the third term represents the commensurability energy. The dimensionless coupling constants C, V_0, and $U_\parallel$ depend on such detailed microscopic structure of the system as the density of states at the Fermi level, the effective electron mass renormalized due to the lattice vibration, the electron-phonon coupling strength, and the cutoff energy.[4]

We now consider interchain tunneling of electrons between nearest-neighboring chains at (x,y) and at (x',y') on the x-y plane, i.e., at the same position z; this gives rise to the interaction of the form $U_\perp\cos(\phi_{\mathbf{r}}-\phi_{\mathbf{r}'})$, where $U_\perp$ is the dimensionless interchain coupling constant and higher-order harmonics have been disregarded. With this included, the Hamiltonian $\mathcal{H}$ for the coupled near-commensurate CDW chains reads

$$\mathcal{H}=\int dz\left\{\sum_{x,y}\left[\frac{p_{\mathbf{r}}^2}{2C}+\frac{U_\parallel}{2}\left(\frac{\partial\phi_{\mathbf{r}}}{\partial z}-\delta_{\mathbf{r}}\right)^2-V_0\cos M\phi_{\mathbf{r}}\right]-\sum_{\langle xy,x'y'\rangle}U_\perp\cos(\phi_{\mathbf{r}}-\phi_{\mathbf{r}'})\right\}, \tag{2}$$

where the *position* $\phi_{\mathbf{r}}$ and the conjugate *momentum* $p_{\mathbf{r}}$ are considered to observe the commutation relation $[\phi_{\mathbf{r}},p_{\mathbf{r}'}]=i\delta_{\mathbf{r},\mathbf{r}'}$, suggesting the position representation $p_{\mathbf{r}}\doteq -i\partial/\partial\phi_{\mathbf{r}}$. In the second summation $\langle xy,x'y'\rangle$ stands for the nearest-neighbor pairs on the x-y plane at fixed z. Throughout this work, we set $\hbar\equiv 1$, $c\equiv 1$, and the Boltzmann constant $k_B\equiv 1$.

Note that in the presence of the commensurability energy, the misfit cannot be simply gauged away and introduces frustration to the system. For the time being we consider the case of strictly commensurate CDW systems without any misfit. To investigate the quantum phase transition in this case, driven by quantum fluctuations at zero temperature, we follow the standard procedure[5] to map a d-dimensional quantum system to a $(d+1)$-dimensional classical system and obtain the corresponding effective action. In Sec. II A, the system with negligible spatial fluctuations along the chain direction is considered and the corresponding effective action at zero temperature is mapped onto the 3D XY model, where commensurability effects are described by the appropriate symmetry-breaking field. Section II B discusses the system in the presence of spatial fluctuations. We first pay attention to the classical limit, where temporal fluctuations may be neglected. Here the system is intrinsically 3D, and the effective action is again mapped onto the 3D XY model. Next, with both spatial and temporal fluctuations considered, the appropriate effective action at zero temperature is identified with the 4D XY model.

A. Homogeneous case

Although it is in general expected that strong fluctuations are present, we for the moment assume that spatial fluctuations along each chain are negligible, which gives a 2D system without z dependence. In the absence of the symmetry-breaking field due to commensurability, Eq. (2) reduces to the 2D XY model with kinetic energy:

$$\mathcal{H}=\sum_{\mathbf{r}}\frac{p_{\mathbf{r}}^2}{2C}-\sum_{\langle\mathbf{r},\mathbf{r}'\rangle}U_\perp\cos(\phi_{\mathbf{r}}-\phi_{\mathbf{r}'}), \tag{3}$$

where the summation in the second term is to be performed over all nearest-neighboring pairs in the 2D space with $\mathbf{r}\equiv(x,y)$. The Hamiltonian in Eq. (3) has been studied in the context of quantum arrays of Josephson junctions.[6] In particular, at zero temperature the 2D quantum system in Eq. (3) is well known to map onto a 3D classical system via the standard lore.[5] Introducing the imaginary time τ axis and dividing the interval between $\tau=0$ and $\tau=T^{-1}$ into N slices of equal width $\Delta\tau=1/NT$, in the zero-temperature limit ($T\to 0$) we arrive at the partition function of the anisotropic 3D XY model:

$$\mathcal{Z}=\oint\mathcal{D}\phi\exp\left[\sum_{\langle\mathbf{r},\mathbf{r}'\rangle}K_{\mathbf{r},\mathbf{r}'}\cos(\phi_{\mathbf{r}}-\phi_{\mathbf{r}'})\right], \tag{4}$$

where $\mathbf{r}\equiv(\tau,x,y)$ represents the position in the 3D space, consisting of the (imaginary) time τ and the 2D space (x,y). The anisotropic coupling is defined on each bond:

$$K_{\mathbf{r},\mathbf{r}'}=\begin{cases}C/\Delta\tau & \text{for } \mathbf{r}'=\mathbf{r}\pm\hat{\boldsymbol{\tau}}\Delta\tau,\\ U_\perp\Delta\tau & \text{for } \mathbf{r}'=\mathbf{r}\pm\hat{\mathbf{x}} \text{ or } \mathbf{r}\pm\hat{\mathbf{y}}.\end{cases}$$

Strictly speaking, we should keep $\Delta\tau$ infinitesimal. Without affecting the universality, however, we can rescale the space and time and obtain the partition function of an isotropic 3D XY model

$$\mathcal{Z}=\oint \mathcal{D}\phi e^{-H}, \tag{5}$$

with the desired effective action

$$-H=K\sum_{\langle \mathbf{r},\mathbf{r}'\rangle}\cos(\phi_{\mathbf{r}}-\phi_{\mathbf{r}'}),$$

where $K^{-1}\equiv(CU_{\perp})^{-1/2}$ measures the amount of quantum fluctuations.

We then accommodate the commensurability effects at zero temperature, taking advantage of the fact that the symmetry-breaking field term is diagonal in the position basis. Via the same procedure and rescaling as in the absence of the symmetry-breaking field, the effective action for the 3D XY model obtains

$$-H=K\sum_{\langle \mathbf{r},\mathbf{r}'\rangle}\cos(\phi_{\mathbf{r}}-\phi_{\mathbf{r}'})+h\sum_{\mathbf{r}}\cos M\phi_{\mathbf{r}}, \tag{6}$$

where the symmetry-breaking field is given by $h\equiv V_0\Delta\tau=V_0\sqrt{C/U_{\perp}}$.

B. General Case

We now turn to the system in which spatial fluctuations in the z direction are present (but still without the misfit), and first consider the case of only spatial fluctuations, with temporal fluctuations negligible. This corresponds to the classical limit in the sense that the momentum and the position decouple and the momentum part, which can be integrated out, does not affect the relevant physics. In this intrinsically 3D case, it is revealing to resort to the discrete formulation and replace the integration $\int dz$ by the summation $\Sigma_z\Delta z$ with sufficiently small Δz. Regarding spatial fluctuation-dependent energy as the continuum form of the cosine interaction in the discrete representation, we obtain from Eq. (2) the effective Hamiltonian for the 3D XY model:

$$-\mathcal{H}=\sum_{\langle \mathbf{r},\mathbf{r}'\rangle}K_{\mathbf{r},\mathbf{r}'}\cos(\phi_{\mathbf{r}}-\phi_{\mathbf{r}'})+h\sum_{\mathbf{r}}\cos M\phi_{\mathbf{r}}, \tag{7}$$

where $\mathbf{r}\equiv(x,y,z)$ represents lattice sites in the 3D space, and the coupling strength and the symmetry-breaking field are given by

$$K_{\mathbf{r},\mathbf{r}'}\equiv\begin{cases}U_{\perp}\Delta z & \text{for } \mathbf{r}'=\mathbf{r}\pm\hat{\mathbf{x}} \text{ or } \mathbf{r}\pm\hat{\mathbf{y}}\\ U_{\parallel}/\Delta z & \text{for } \mathbf{r}'=\mathbf{r}\pm\hat{\mathbf{z}}\Delta z\end{cases}$$

$$h\equiv V_0\Delta z.$$

Interestingly enough, Eqs. (6) and (7) show that both the (zero-temperature) quantum phase transition in the absence of spatial fluctuations and the (finite-temperature) classical phase transition in the absence of temporal fluctuations are described by the same 3D XY model under symmetry-breaking fields. Quantum fluctuations in the former play the role of thermal fluctuations in the latter, tending to restore symmetry.

We finally consider the general case, where both spatial and temporal fluctuations are significant. Adding the kinetic-energy term to the 3D effective action in Eq. (7) and following the same procedure as that in Sec. II A at zero temperature, we obtain the 4D XY model with the effective action

$$-H=\sum_{\langle i,i'\rangle}\mathcal{K}_{i,i'}\cos(\phi_i-\phi_{i'})+h\sum_i\cos M\phi_i, \tag{8}$$

where $i\equiv(\tau,x,y,z)$ denotes 4D space-time lattice sites and the anisotropic coupling and the symmetry-breaking field are given by

$$\mathcal{K}_{i,i'}\equiv\begin{cases}\dfrac{\Delta\tau}{\Delta z}U_{\parallel} & \text{for } i'=i\pm\hat{\mathbf{z}}\Delta z\\ \dfrac{C}{\Delta z\Delta\tau} & \text{for } i'=i\pm\hat{\boldsymbol{\tau}}\Delta\tau\\ \Delta z\Delta\tau U_{\perp} & \text{for other nearest neighbors,}\end{cases}$$

$$h\equiv V_0\Delta z\Delta\tau.$$

In this manner, the coupled near-commensurate CDW systems (without misfit) can be described by the appropriate XY models under symmetry-breaking fields. Depending on whether spatial and/or temporal fluctuations are present, the effective dimension of the system is determined to be three or four: It is four if both fluctuations are significant at zero temperature and three otherwise. The commensurability effects are described by the symmetry-breaking field, which introduces Z_M symmetry to the system. Such a symmetry-breaking field affects the ground-state symmetry and is expected to be relevant in the sense of the renormalization-group (RG) theory. In the limit $M\to\infty$, however, the Z_M symmetry is hardly distinguishable from the underlying U(1) symmetry in the XY model. Therefore we expect the phase transition to be crucially dependent upon the commensurability factor M, and devote the following two sections to the investigation of the phase transitions in the 3D and 4D XY models under symmetry-breaking fields.

III. 3D XY MODEL UNDER SYMMETRY-BREAKING FIELD

In this section we investigate the phase transition in the 3D XY model whose effective action is given by Eq. (6). In the absence of the symmetry-breaking field ($h=0$), the 3D XY model has been studied both analytically[7–9] and numerically,[10] revealing that vortex loops do exist and proliferate at the phase transition. Accordingly, the topological scaling idea has been extended to the 3D transition with conventional long-range order, with the scaling procedure of Ref. 11 generalized appropriately for 3D directed loops.[8,9] One may then be tempted to extend the study of the 2D model in Ref. 12 to incorporate the symmetry-breaking term in the 3D XY model, and combine recursion relations for the

vortex fugacity y_0 and the field perturbation y_h according to the duality relation between them. However, in contrast to the 2D case, the geometric scaling of the coupling constant in three dimensions results in nonzero values of y_0 and y_h at the fixed point.[9]

On the other hand, the ϵ expansion[13] is well known to provide a mathematical formalism for calculating critical exponents of the O(n) model near four spatial dimensions, allowing classification of the universality class of the system. Here we extend the ϵ expansion approach to incorporate the effects of the symmetry-breaking field. The ϵ expansion turns out to be useful only for small commensurability factor M; we thus supplement its limitations with the Monte Carlo numerical method. In Sec. III A, the symmetry-breaking perturbation is treated within the ϵ expansion and Sec. III B is devoted to the Monte Carlo simulations of the 3D XY model under symmetry-breaking fields.

A. ϵ Expansion

We consider the ϵ expansion for the 3D XY model, extending the original formulation for the O(n) model[13] to incorporate the symmetry-breaking field. To begin with, we employ the two-component continuous local variable or spin $\mathbf{S_r}=(S^x_\mathbf{r},S^y_\mathbf{r})$ at each 3D lattice site $\mathbf{r}$, the total number of which is denoted by N. The constraint that each spin has the unit magnitude is relaxed by the additional weight factor introduced to the partition function

$$\mathcal{Z}=\left(\prod_\mathbf{r}\int_{-\infty}^{\infty}d\mathbf{S_r}\right)e^{-[H+W(\mathbf{S_r})]}, \tag{9}$$

with the weight factor ($u>0$)

$$\exp[-W(\mathbf{S})]=\exp\left[-\frac{1}{2}bS^2-uS^4\right],$$

which has been expanded up to $O(S^4)$. At the physical XY fixed point the sixth-order term is less relevant in dimension $d=4-\epsilon$ than $d=4$.[14] With the identification $S^x_\mathbf{r}=\cos\phi_\mathbf{r}$ and $S^y_\mathbf{r}=\sin\phi_\mathbf{r}$, the original action in Eq. (6) is written in terms of the continuous spin $\mathbf{S_r}$:

$$-H=\sum_{\mathbf{r},\mathbf{r}'}K\mathbf{S_r}\cdot\mathbf{S_{r'}}+\frac{h}{2}\sum_\mathbf{r}\left[(2S^x_\mathbf{r})^M-\frac{M}{1!}(2S^x_\mathbf{r})^{M-2}+\frac{M(M-3)}{2!}(2S^x_\mathbf{r})^{M-4}-\cdots\right]. \tag{10}$$

Note that for $M<4$ the order of the action does not exceed $O(S^4)$, leading to the Ginzburg-Landau-Wilson (GLW) effective Hamiltonian $\mathcal{H}=H+W$ to $O(S^4)$.

We first examine the case $M=2$. In the momentum space representation, keeping only relevant terms to $O(q^2)$ and scaling the spin variable according to $\mathbf{S_q}=(Ka^{d+2})^{-1/2}\boldsymbol{\sigma}_\mathbf{q}$, we express the GLW Hamiltonian as

$$\begin{aligned}-\mathcal{H}=&-\frac{1}{2}\int_\mathbf{q}(r_x+q^2)\sigma^x_\mathbf{q}\sigma^x_{-\mathbf{q}}-\frac{1}{2}\int_\mathbf{q}(r_y+q^2)\sigma^y_\mathbf{q}\sigma^y_{-\mathbf{q}}\\&+V_1\int_\mathbf{q}\int_{\mathbf{q}'}\int_{\mathbf{q}''}\sigma^x_\mathbf{q}\sigma^x_{\mathbf{q}'}\sigma^x_{\mathbf{q}''}\sigma^x_{-\mathbf{q}-\mathbf{q}'-\mathbf{q}''}\\&+2V_2\int_\mathbf{q}\int_{\mathbf{q}'}\int_{\mathbf{q}''}\sigma^x_\mathbf{q}\sigma^x_{\mathbf{q}'}\sigma^y_{\mathbf{q}''}\sigma^y_{-\mathbf{q}-\mathbf{q}'-\mathbf{q}''}\\&+V_3\int_\mathbf{q}\int_{\mathbf{q}'}\int_{\mathbf{q}''}\sigma^y_\mathbf{q}\sigma^y_{\mathbf{q}'}\sigma^y_{\mathbf{q}''}\sigma^y_{-\mathbf{q}-\mathbf{q}'-\mathbf{q}''},\end{aligned} \tag{11}$$

where the coefficients are given by

$$r_x=\frac{1}{Ka^2}(b-dK-2h),$$

$$r_y=\frac{1}{Ka^2}(b-dK),$$

$$V_1=V_2=V_3=-u<0,$$

and $\int_\mathbf{q}\equiv\int d\mathbf{q}/(2\pi)^d=(1/Na^d)\Sigma_\mathbf{q}$ with the lattice constant a restored for clarity. Here it is shown that the $M=2$ symmetry-breaking field gives rise to anisotropy in the quadratic term, making r_x less than r_y. Following the standard procedure, we obtain the recursion relations to the leading order in $\epsilon\equiv4-d$:

$$\begin{aligned}\frac{\partial r_x}{\partial l}&=2r_x-\frac{12C}{1+r_x}V_1-\frac{4C}{1+r_y}V_2,\\\frac{\partial r_y}{\partial l}&=2r_y-\frac{4C}{1+r_x}V_2-\frac{12C}{1+r_y}V_3,\\\frac{\partial V_1}{\partial l}&=\epsilon V_1+\frac{36C}{(1+r_x)^2}V_1^2+\frac{4C}{(1+r_y)^2}V_2^2,\\\frac{\partial V_2}{\partial l}&=\epsilon V_2+\frac{16C}{(1+r_x)(1+r_y)}V_2^2+\frac{12C}{(1+r_x)(1+r_y)}V_1V_2\\&\quad+\frac{12C}{(1+r_x)(1+r_y)}V_2V_3,\\\frac{\partial V_3}{\partial l}&=\epsilon V_3+\frac{36C}{(1+r_x)^2}V_3^2+\frac{4C}{(1+r_y)^2}V_2^2,\end{aligned} \tag{12}$$

with the spatial scale factor l and $C\equiv2^{1-d}\pi^{d/2}/(d/2-1)!$.

In the absence of the symmetry-breaking field ($h=0$), the parameter space reduces to the 2D space (r,V) since $r_x=r_y\equiv r$ and $V_1=V_2=V_3\equiv V$. In this case the nontrivial fixed point of the recursion relation in Eq. (12) is simply the XY fixed point, given by

$$r^*=-\frac{\epsilon}{5},\quad V^*=-\frac{\epsilon}{40C} \tag{13}$$

to $O(\epsilon)$. As the symmetry-breaking field is turned on, however, we have $r_x < r_y$ at the initial locus and need to examine the RG flow in the full 5D parameter space $(r_x, r_y, V_1, V_2, V_3)$. To investigate the stability of the XY fixed point in the 5D parameter space, we linearize Eq. (12) about this point and obtain a stability matrix which yields five eigenvalues together with corresponding scaling exponents:

$$y_1 = 2 - \frac{\epsilon}{5}, \quad y_2 = 2 - \frac{2\epsilon}{5},$$

$$y_3 = -\epsilon, \quad y_4 = -\frac{\epsilon}{5}, \quad y_5 = -\frac{4\epsilon}{5}. \tag{14}$$

Since the exponents y_3, y_4, and y_5, which correspond to the three eigenvectors spanning the 3D subspace (V_1, V_2, V_3), are all strictly negative, it is concluded that all V_i's (for $i = 1,2,3$) are irrelevant at the XY fixed point. In contrast, both y_1 and y_2 are positive, indicating that the XY fixed point is unstable in the 2D subspace (r_x, r_y). The initial locus, which is kept off the XY fixed point by the symmetry-breaking field, should flow far off the XY fixed point. Instead it is expected to flow toward the Ising fixed point located at

$$r_x^* = -\frac{\epsilon}{6}, \quad r_y^* = \infty, \quad V_1^* = -\frac{\epsilon}{36C}, \quad V_2^* = V_3^* = 0. \tag{15}$$

At this point it is more appropriate to take r_y^{-1} as the scaling field, giving the scaling exponents

$$y_{r_x} = 2 - \frac{\epsilon}{3}, \quad y_{r_y^{-1}} = -2. \tag{16}$$

Thus the initial locus with $r_x < r_y$ indeed flows toward the Ising fixed point along the stable r_y direction. In this manner, the symmetry-breaking field for $M = 2$ introduces anisotropy in the quadratic term, making the XY fixed point unstable and generating an Ising or two-state clock fixed point. Revealed accordingly is a single second-order transition between two-state clock order and disorder.

We next turn to the case $M = 3$, where Eq. (10) shows that terms of linear and third order in the x component of the spin come into play; power counting suggests that these fields are relevant near $d = 4$. Owing to the anisotropy associated with the absence of S^y terms, in particular, the cubic term $(S^x)^3$ here may not be removed by mere shift and is not redundant, in contrast to the case of the Ising model. The symmetry-breaking field is thus expected to drive the transition between the disordered phase and the three-state clock ordered phase.

Finally the symmetry-breaking field for $M = 4$ introduces anisotropy in the quartic term:

$$V_1 = -u + 8a^{d-4}K^{-2}h,$$

$$V_2 = V_3 = -u. \tag{17}$$

This leads the action in Eq. (11) to be unstable for sufficiently large values of the field h, making it necessary to consider higher-order terms in the weight function $W(\mathbf{S})$ for stability. Unfortunately, such calculation of higher cumulants is quite a formidable job, and it is very difficult to extend the ϵ expansion to the case of a high commensurability factor.

B. Monte Carlo simulations

This section presents the Monte Carlo study of the 3D XY model in symmetry-breaking fields. To estimate the critical temperatures and determine critical exponents, we have performed Monte Carlo simulations at "temperatures" (i.e., quantum or temporal fluctuations) ranging from $K^{-1} = 0.5$ to $K^{-1} = 5$ on lattices of linear size $L = 4$ up to $L = 32$ for several commensurability factors and field strengths. Measured in simulations are the order parameter m and the susceptibility χ defined to be

$$m \equiv \left\langle \left| \frac{1}{N} \sum_{\mathbf{r}} e^{i\phi_{\mathbf{r}}} \right| \right\rangle,$$

$$\chi \equiv \left\langle \left| \frac{1}{N} \sum_{\mathbf{r}} e^{i\phi_{\mathbf{r}}} \right|^2 \right\rangle - \left\langle \left| \frac{1}{N} \sum_{\mathbf{r}} e^{i\phi_{\mathbf{r}}} \right| \right\rangle^2, \tag{18}$$

where N is the number of sites. We have employed the multiple histogram method[15] to interpolate the quantities calculated sparsely in a given range of the temperature to any temperature inside the range. It not only saves a great deal of computing time but also provides the values of quantities at arbitrary temperatures for finite-size scaling, resulting in critical exponents of better accuracy. In fact we have obtained the best collapse of the scaling function such as

$$\tilde{m}(L^{1/\nu}t) = L^{\beta/\nu}m(t), \tag{19}$$

with the reduced temperature $t \equiv T/T_c - 1 \equiv K_c/K - 1$, by minimizing the measure of error[15]

$$\sigma_m^2 \equiv \frac{1}{x_{max} - x_{min}} \int_{x_{min}}^{x_{max}} dx [\langle\langle \tilde{m}^2(x) \rangle\rangle - \langle\langle \tilde{m}(x) \rangle\rangle^2] \tag{20}$$

over the critical temperature and exponents. Here $\langle\langle \cdots \rangle\rangle$ stands for the average over the lattice size and similar relations for the susceptibility have also been considered. We have taken the range $[x_{min}, x_{max}] = [-\Delta x, \Delta x]$ and attempted a series of collapses as Δx is diminished. The result has then been extrapolated to the limit $\Delta x \to 0$.

Figure 1 presents typical collapse of the scaling function with the best-estimated critical temperature T_c and exponents β and ν; nice collapse behavior can be observed near the critical temperature $(t = 0)$. The inset in Fig. 1 discloses how the corresponding error σ_m^2 depends on the value of the exponent ν. We have thus estimated the error in the obtained critical exponent from the standard deviation of the minimizing values over the sample ensemble. In this way, the phase transition for $M = 2$ is found to be of the second order with the critical exponents $\nu = 0.63 \pm 0.01$ and $\beta = 0.34 \pm 0.04$ for $h = 1.2$ and $\nu = 0.627 \pm 0.004$ and $\beta = 0.32 \pm 0.01$ for $h = 2.7$. These results coincide perfectly with the known critical exponents for the 3D Ising model: $\nu = 0.630$ and $\beta = 0.324$, thus demonstrating the validity of the ϵ expansion

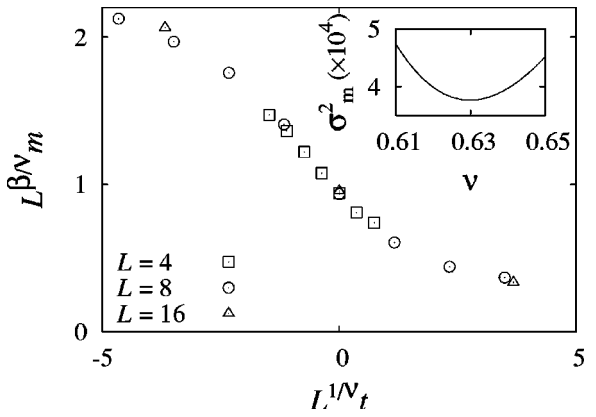

FIG. 1. Data collapse of the order parameter m for three different values of the system size L, with the best-estimated critical temperature and exponents given in the text. The inset shows the dependence of the error σ_m^2 on the value of ν, with T_c and β fixed at their best-estimated values. The data have been taken for $M=2$ and at $h=2.7$; typical error bars are not larger than the symbol sizes.

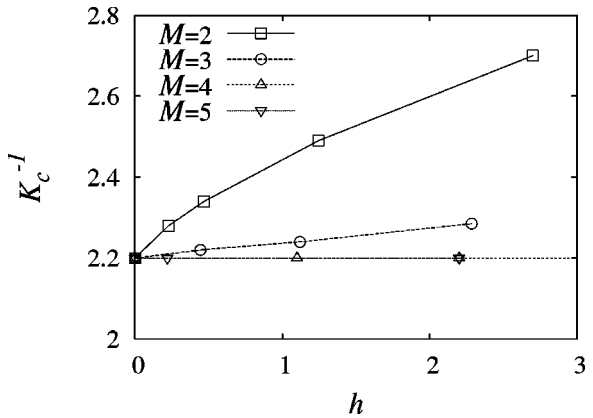

FIG. 2. Critical temperature K_c^{-1} in the 3D XY model under symmetry-breaking fields vs the symmetry-breaking field strength h, for the commensurability factor $M=2,3,4$, and 5. Typical error bars are smaller than the symbol size and lines are merely guides to eyes.

analysis in Sec. III A. Here it is of interest that the same universality class was also reported in the quantum Monte Carlo study of a tight-binding model of spinless fermion chains coupled by intrachain and interchain Coulomb interactions.[16] The tight-binding model analysis, though being restricted to the $M=2$ case, could incorporate amplitude fluctuations of the CDW order parameter directly. Indeed the accordance between the two analyses manifests that fluctuations in the phase (rather than in the amplitude) mostly determine the nature of the transition.

For $M=3$, on the other hand, we have found no evidence for the first-order transition, and obtained the estimation $\nu=0.596\pm0.007$ and $\beta=0.3\pm0.01$; this is to be compared with the long-standing controversy as to whether the transition in the 3D three-state Potts model is of the first order or continuous.[17] It is also of interest that the critical behavior for $M\geqslant4$ is similar to that of the 3D XY model without any symmetry-breaking field. Figure 2 shows the critical temperature (i.e., the critical fluctuation strength) K_c versus the field strength h for $2\leqslant M\leqslant5$. It is observed that for $M\leqslant3$ the critical temperature increases with the field strength while for $M\geqslant4$ the commensurability energy appears to have no effect on the critical temperature, in the range probed. Such critical behavior for $M\geqslant4$, similar to that of the ordinary 3D XY model, reflects that, as noted in Sec. II, the Z_M symmetry for large M is indiscernible from the U(1) symmetry underlying in the XY model.

IV. 4D XY MODEL UNDER SYMMETRY-BREAKING FIELD

We now study the phase transition in the 4D XY model, described by the effective action in Eq. (8), through the use of the mean-field approximation. Here the mean-field approximation, developed for superconducting arrays in applied magnetic fields,[18] is expected to be accurate since the upper critical dimension of the XY model is given by $d_u=4$. With the space and time rescaled appropriately, the (mean-field) self-consistent equation reads

$$\langle e^{i\phi}\rangle=\mathcal{Z}_{MF}^{-1}\int_0^{2\pi}d\phi e^{i\phi}e^{-H_{MF}}, \tag{21}$$

where $\mathcal{Z}_{MF}$ is the partition function,

$$\mathcal{Z}_{MF}=\int_0^{2\pi}d\phi\, e^{-H_{MF}}$$

corresponding to the mean-field action

$$-H_{MF}=4K(\langle\cos\phi\rangle\cos\phi+\langle\sin\phi\rangle)\sin\phi+h\cos M\,\phi, \tag{22}$$

with the rescaled coupling constant $K\equiv\sqrt{CU_\perp}$ and field $h\equiv V_0\sqrt{C/U_\perp}$.

In the absence of the symmetry-breaking field, the self-consistent equation leads to the equation of state for the order parameter $m\equiv\sqrt{\langle\cos\phi\rangle^2+\langle\sin\phi\rangle^2}$:

$$m=\frac{I_1(4Km)}{I_0(4Km)}, \tag{23}$$

where I_n is the nth modified Bessel function. The system is in the disordered phase for $K<K_c(h=0)=1/2$ characterized by $m=0$; beyond $K_c(h=0)$ the ordered phase with $m\neq0$ is favored. Similarly, the $M=1$ case can be analyzed easily, where arbitrarily small but positive h results in $\langle\cos\phi\rangle>0$ and $\langle\sin\phi\rangle=0$. The equation of state is thus

$$\langle\cos\phi\rangle=\frac{I_1(4K\langle\cos\phi\rangle+h)}{I_0(4K\langle\cos\phi\rangle+h)}. \tag{24}$$

For larger values of M, Eq. (21) may be solved numerically with the parameters K and h varied. It is found that there exists a field-dependent transition coupling strength $K_c(h)$ below which Eq. (21) bears only the null solution $\langle\cos\phi\rangle=\langle\sin\phi\rangle=0$. As K is increased beyond $K_c(h)$, nonzero stable solutions emerge. Due to the Z_M symmetry, i.e.,

the invariance of the action under the shift in the angle by $2\pi n/M$ for any integer n, the solution of Eq. (21) can be expressed in terms of the M-state clock order parameter $m(K,h)$:

$$\langle e^{i\phi}\rangle = m(K,h)e^{2\pi i n/M}, \tag{25}$$

with integer $n=0,1,\ldots,M-1$. The critical coupling strength $K_c(h)$ is defined to be the largest value of K satisfying $m(K,h)=0$.

Figure 3 shows how the order parameter m depends on the parameters K and h for different values of M. It is observed that m in general increases rapidly from zero as K exceeds K_c and then saturates to unity, with the increase more rapid for larger h. While for $M=2$ and $M\geqslant 4$ the transition is found to be of the second order, numerical results for $M=3$ indicate a first-order transition, which is expected from the appearance of the third-order term in the ϵ expansion. For $M\leqslant 3$, the critical coupling strength $K_c(h)$, starting from $K_c(h=0)=1/2$, decreases with h almost exponentially to the asymptotic values, 0.250 and 0.462 for $M=2$ and for $M=3$, respectively. For $M\geqslant 4$, on the other hand, the transition point does not depend on the strength of the symmetry-breaking field, giving $K_c=1/2$ regardless of h. Again manifested is the crucial role of commensurability in the phase transition.

The resulting phase diagram for the 4D XY model under the symmetry-breaking field is displayed in Fig. 4, where the boundary K_c^{-1} versus h is plotted for different values of M. When $K^{-1}<K_c^{-1}$, the Z_M symmetry as well as the U(1) symmetry is broken and identified is the M-state clock ordered phase, with one of the minima of $-h\cos M\phi$ favored. When $K^{-1}>K_c^{-1}$, unlike the U(1) symmetry broken explicitly for $h\neq 0$, the Z_M symmetry remains unbroken, leading to the disordered phase.

V. COMMENSURATE-INCOMMENSURATE TRANSITION

Up to the present, we have assumed the absence of misfit, so that only the transition between the disordered phase and the M-state clock ordered phase, where commensurate CDW's are developed, has been considered in several idealized cases described in Sec. II. However, the misfit, being a key ingredient to bring about the commensurate-incommensurate transition in a near-commensurate CDW chain, must be taken into consideration in understanding various transitions in the coupled CDW system.

It is well known from the study of the 1D Frenkel-Kontorova model[19] at zero temperature that a single near-commensurate CDW changes from the commensurate state to the incommensurate state when the misfit exceeds a critical value depending on the commensurability energy. At finite temperatures the 1D CDW system is always in the incommensurate state.[20] On the other hand, in the coupled CDW system, interactions between the CDW chains may alter the nature of the transition. First of all, the effective dimensions of the system grow to three, giving rise to the persistence of long-range order, as observed in the previous sections. Moreover, the CI transition itself can also be affected by the interchain coupling in that the interactions favor either the commensurate state or the incommensurate state, as explained below. To investigate the phase transition of the coupled CDW system, we consider the Hamiltonian in Eq. (2) without temporal fluctuations, which makes the problem simpler and allows us to focus on the static properties only.

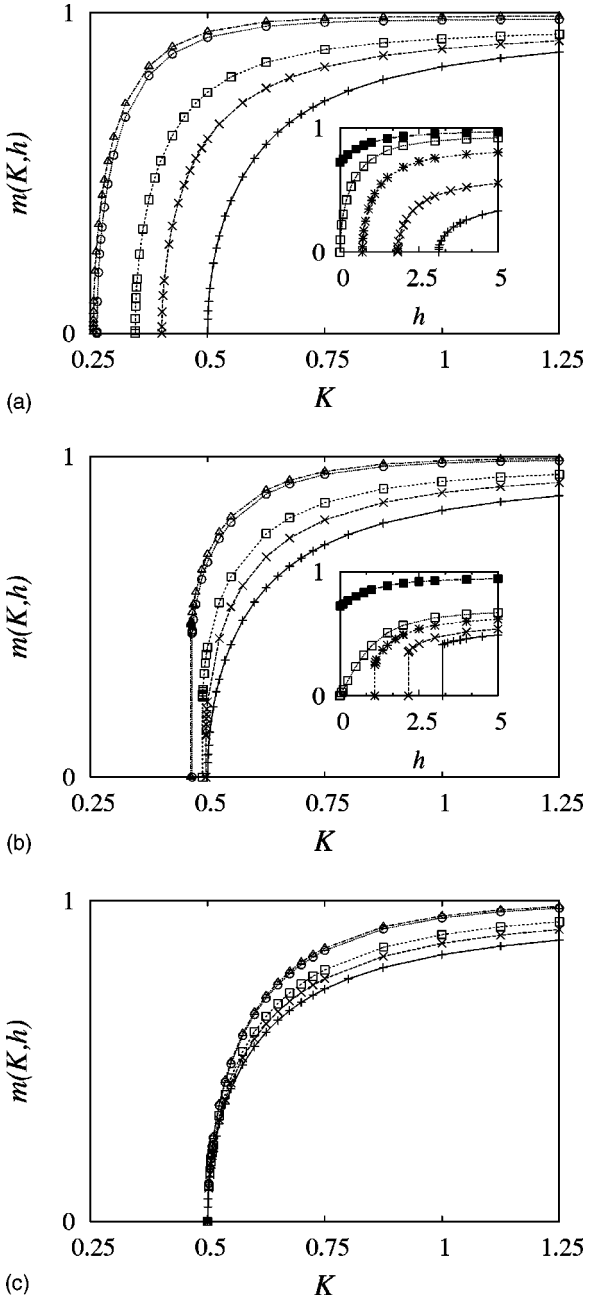

FIG. 3. Order parameter m as a function of the coupling K and the field strength h for (a) $M=2$, (b) $M=3$, and (c) $M=4$. Main graphs show m vs K for $h=0(+),0.5(\times),1(\square),5(\circ)$, and $10(\triangle)$ from below. Insets display $m(K,h)$ vs h for various values of K: From below (a) $K=0.275,0.3,0.375,0.5$, and 0.75; (b) $K=0.47,0.475,0.4875,0.5$, and 0.75. The overall behavior of the order parameter for $M>4$ is the same as that for $M=4$.

At zero temperature the problem is rather simple to solve.

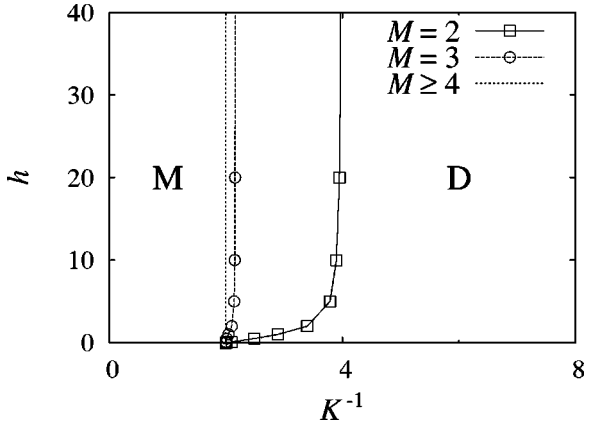

FIG. 4. Phase diagram for the 4D *XY* model under the symmetry-breaking field, displaying the boundaries between the *M*-state clock order phase (M) and the disordered phase (D) for different values of *M*. Lines for $M=2$ and 3 are merely guides to eyes.

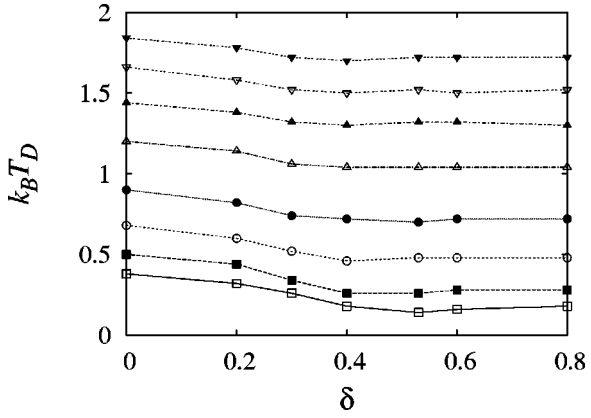

FIG. 5. Behavior of the order-disorder transition temperature T_D with the misfit δ in the $M=2$ coupled CDW system for $U_{\parallel}=1$ and $V_0=0.2$. Each symbol corresponds to a different value of the interchain coupling strength: $U_{\perp}=0.01(\square),0.02(\blacksquare),0.05(\bigcirc),0.1(\bullet)$, $0.2(\triangle),0.3(\blacktriangle),0.4(\nabla)$, and $0.5(\blacktriangledown)$. Typical error bars are smaller than the symbol sizes and lines are merely guides to eyes.

The interchain coupling term in Eq. (2) reaches the minimum when all the phases $\phi_{\mathbf{r}}$ in the *xy* plane become equal to each other. All the CDW chains, therefore, follow the same phase configurations determined by the 1D Frenkel-Kontorova model, thus undergo the CI transition at the critical misfit given by[19]

$$\delta_c=\frac{4}{\pi}\sqrt{\frac{V_0}{U_{\parallel}}}, \tag{26}$$

regardless of the interchain coupling strength $U_{\perp}$.

The system at finite temperatures is examined by means of the Monte Carlo method. For this we discretize the *z* axis in Eq. (2) as in Sec. II B, and obtain the lattice Hamiltonian

$$\mathcal{H}=\sum_{\mathbf{r}}\frac{U_{\parallel}}{2}(\phi_{\mathbf{r}+\mathbf{z}}-\phi_{\mathbf{r}}-\delta)^2-\sum_{\mathbf{r}}V_0\cos M\phi_{\mathbf{r}}$$

$$-\sum_{z}\sum_{\langle xy,x'y'\rangle}U_{\perp}\cos(\phi_{\mathbf{r}}-\phi_{\mathbf{r}'}), \tag{27}$$

where Δz has been absorbed into the coupling constants. Since the dimension along the CDW chain is usually longer than the lateral dimensions, the lattice size L_z along the *z* axis is kept to be two times larger than the other linear sizes in our simulations, and accordingly the interchain coupling $U_{\perp}$ is restricted to be smaller than $U_{\parallel}$ to avoid inessential finite-size effects. We further set the parameters to $U_{\parallel}=1$ and $V_0=0.2$ and sweep the interchain coupling strength from 0.01 to 0.5 and the misfit δ, which is assumed to be uniform throughout the system, from zero to 0.8 beyond the critical misfit $\delta_c(=0.569)$.

The order-disorder transition is described conveniently by the (incommensurate) order parameter defined to be

$$m\equiv\left\langle\left|\frac{1}{N}\sum_{\mathbf{r}}e^{i(\phi_{\mathbf{r}}-\delta z)}\right|\right\rangle \tag{28}$$

and its susceptibility χ. Note that in the thermodynamic limit this order parameter vanishes not only in the disordered phase but also in the commensurate phase; in the system of finite size it may remain nonzero even in the perfectly commensurate state. We also compute the soliton density ρ_s,[21] i.e., the soliton number per site per chain, which characterizes the CI transition. For the detection of any hysteresis, these two physical quantities have been measured in two different ways: in the cooling-down process with randomized initial phase configurations and in the heating-up process starting from the zero-temperature ground state. In each process the system has been equilibrated sufficiently while the temperature is varied gradually.

Shown in Fig. 5 is the dependence of the order-disorder transition temperature T_D on the misfit δ in the $M=2$ CDW system at various interchain coupling strengths. It is observed that the misfit tends to reduce the transition temperature: The transition temperature first decreases as the misfit is increased from zero, then saturates when the misfit reaches a value comparable to δ_c. Here stronger interchain coupling, which helps to increase the transition temperature, in general weakens the effects of the misfit. Besides the transition temperatures, the critical exponents also change with the misfit. For instance, the critical exponents in the system with $U_{\perp}=0.1$ are found to be $\nu=0.79\pm0.02$ and $\gamma=1.33\pm0.01$ at $\delta=0.2$; $\nu=0.77\pm0.03$ and $\gamma=1.64\pm0.05$ at $\delta=0.4$. This suggests that the introduction of the misfit changes the nature of the ordered phase, making it different from the 3D *XY* ordered phase. It should be identified as the incommensurate CDW phase, as demonstrated below.

We now draw our attention to the CI transition occurring at lower temperatures. In the absence of misfit ($\delta=0$) the soliton density ρ_s is observed to vanish on average at all temperatures below T_D, indicating that the CDW's formed are commensurate even in the presence of thermal fluctuations. Such a commensurate phase is destroyed by the introduction of misfit, even for $\delta<\delta_c$, with the help of thermal fluctuations. Figure 6 exhibits the behaviors of the order parameter and of the soliton density as the temperature is varied in the system with misfit $\delta=0.2$. It is shown that the

order parameter reaches its maximum at temperature near T_D and decreases to zero as the temperature is reduced while the soliton density begins to decrease from its maximum value at $T \approx T_D$ and vanishes almost to zero at very low temperatures. Nonzero values of the order parameter and of the soliton density together in the regime $T \lesssim T_D$ correspond to the formation of incommensurate CDW's. Thus the order-disorder transition at $T = T_D$ is identified as the transition between the incommensurate CDW state and the disordered state. In addition, the vanishing soliton density (see the inset in Fig. 6) is a sign of the commensurate CDW phase; this indicates the presence of a CI transition driven by thermal fluctuations. The CI transition temperature T_{IC} is defined to be the temperature at which the soliton density begins to be nonzero (in the thermodynamic limit). Although our computing ability disallows us to determine the precise value of T_{IC}, Fig. 6(b) manifests that T_{IC} increases with the interchain coupling strength. In this sense the interchain interactions favor the commensurate state. In contrast, it is also observed that the interchain interactions prefer the incommensurate state at the misfit values somewhat larger (but still smaller than δ_c).

Figure 7 compares the order parameter and the soliton density at $\delta = 0.4$, measured in two different processes: the cooling process and the heating one. Unlike the case $\delta = 0.2$, a hysteresis is evident at $\delta = 0.4$ (and also in the undisplayed case of $\delta = 0.3$), as shown in Figs. 7(a) and 7(b) for the order parameter and in Fig. 7(c) and Fig. 7(d) for the soliton density. In the heating process starting from the commensurate ground state at zero temperature, the commensurate CDW's survive some thermal fluctuations and experience the CI transition at a finite transition temperature. In contrast, as the temperature is lowered in the cooling process, the order parameter keeps increasing and the soliton density saturates to a finite value, unless the interchain coupling is sufficiently weak (i.e., for $U_\perp > 0.02$). This implies that the system still consists of the incommensurate CDW's at temperatures where commensurate CDW's are supposed to be more stable. For weak coupling ($U_\perp \leqslant 0.02$), on the other hand, no discrepancy between the two processes is observed.

It is of interest to compare the hysteresis observed here with the one reported in the specific heat around the CI transition in a number of incommensurate systems.[22] The latter is attributed to the effects of pinning of the incommensurate modulation due to defects or impurities; our observation, in contrast, shows that the hysteresis can appear even in the absence of defects, for which interchain interactions are responsible. Namely, the interchain coupling operates in different ways depending on the process: In the cooling process, correlations between CDW chains due to the interchain interactions hinder each CDW chain from getting into the commensurate state. On the contrary, in the heating process, the interchain correlations hold each chain close to the zero-temperature ground state until thermal fluctuations become comparable to the interchain interaction energy. This argument is supported by the observation that the order parameter and the soliton density increase abruptly in a narrow region of the temperature, as shown in Figs. 7(b) and 7(d), and such discrepancy becomes manifest as the interchain coupling becomes stronger. In addition, in the same narrow region the soliton number and the order parameter fluctuate strongly while the energy fluctuations are relatively weak. This suggests a kind of configurational fluctuations over many metastable states.

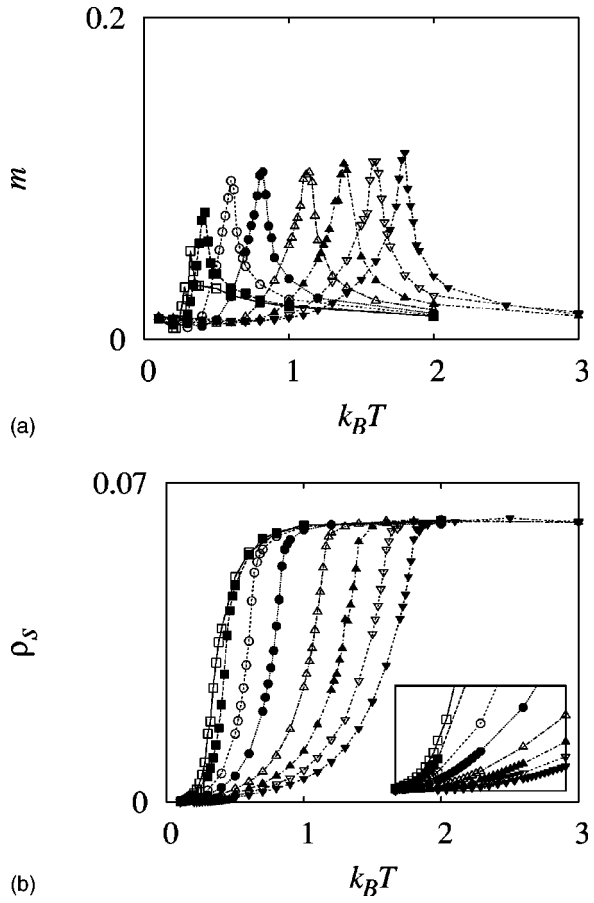

FIG. 6. (a) The order parameter m and (b) the soliton density ρ_s vs the temperature T in the $M = 2$ system of misfit $\delta = 0.2$ and size $L_z = 32$. Each symbol corresponds to a different value of the interchain coupling strength as listed in Fig. 5. The inset is an enlarged view of the soliton density in the range $0.1 \leqslant T \leqslant 0.5$.

For large values of the misfit ($\delta \gtrsim \delta_c$), neither commensurate CDW nor hysteresis is observed and the soliton density does not vanish even at zero temperature in any process. Only the transition separating the incommensurate CDW state from the disordered state is thus identified.

We have also performed similar simulations for the commensurability factor $M = 3$, only to obtain results qualitatively the same as those for $M = 2$ presented above. Quantitative differences observed include that for $M = 3$ the misfit affects the transition temperature more weakly and the hysteresis takes place even at smaller misfit such as $\delta = 0.2$.

VI. PHASE DIAGRAM

Combining the results for the 3D and 4D XY models under symmetry-breaking fields, studied in Secs. III and IV, and those for the near-commensurate CDW model, studied in Sec. V, we are ready to describe the phase transition in the

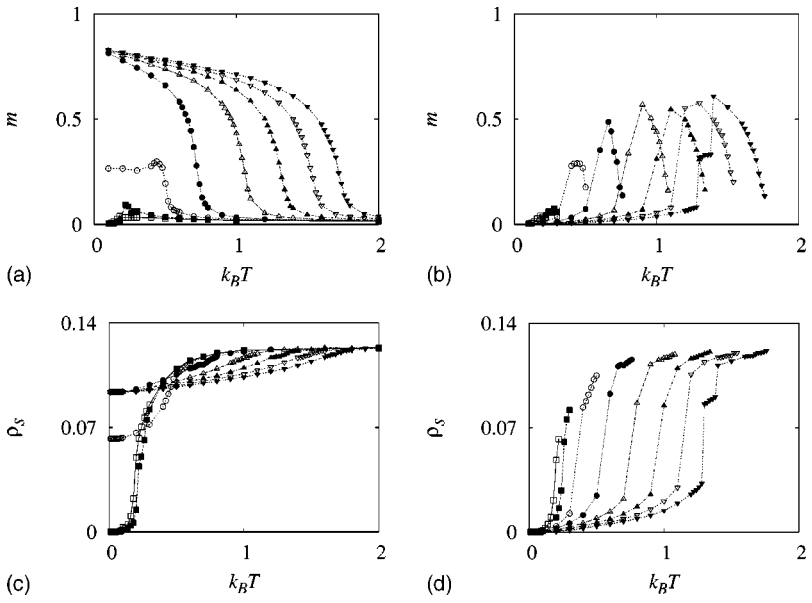

FIG. 7. The order parameter m [(a) and (b)] and the soliton density ρ_s [(c) and (d)] vs the temperature T in the $M=2$ system of misfit $\delta=0.4$ and size $L_z=32$. The left figures [(a) and (c)] and the right ones [(b) and (d)] show the data obtained in the cooling process and in the heating process, respectively. Each symbol corresponds to a different value of the interchain coupling strength as listed in Fig. 5.

coupled CDW system. First, we focus on the system in the absence of any misfit ($\delta=0$). For this purpose, it is adequate to consider the 3D space consisting of the three parameters: the temperature T, the strength of the symmetry-breaking field h, and the amount of quantum or temporal fluctuations K^{-1}. On each of the three planes ($T=0$, $K^{-1}=0$, and $h=0$) in the 3D space, appropriate boundaries separating various phases can be plotted through the use of the known results, as shown in Fig. 8. The phase at a given point in the 3D space can then be speculated by means of finite-size scaling in the region near $T=0$ or the semi-classical methods in the $K^{-1}\approx 0$ region.

We first consider the homogeneous case, where spatial fluctuations along each chain are negligible, and show the phase diagram in Fig. 8 for (a) $M=4$ and (b) $M\geqslant 5$. At zero temperature, the system is mapped onto the 3D XY model as discussed in Sec. II, and the corresponding phase diagram, obtained in Sec. III, is sketched on the h-K^{-1} plane. On the other hand, in the absence of temporal fluctuations ($K^{-1}=0$), the system maps onto the classical 2D XY model under symmetry-breaking fields, for which the phase diagram in Ref. 12 is drawn on the h-T plane. Finally, on the T-K^{-1} plane with $h=0$, the system is described by the Hamiltonian in Eq. (3) and expected to display the Berezinskii-Kosterlitz-Thouless transition renormalized by quantum fluctuations.[6,23] Note that the cases $M=2$ and 3 are not shown here. In this case presumably Ising/Potts critical lines exist on the h-T plane; however, it is not known how these lines connect up to the phase boundary for $h=0$.

In the general case with spatial fluctuations present, we obtain the phase diagram shown in Figs. 8(c) and 8(d) for $M\leqslant 3$ and $M\geqslant 4$, respectively. Owing to the additional dimension along the chain direction, the system maps onto the 3D XY model in the classical limit, i.e., on the h-T plane, whereas 4D XY model is obtained at zero temperature. Accordingly, on the h-K^{-1} plane, the phase diagram of the 4D XY model obtained in Sec. IV is drawn. It is observed that the 3D XY ordered phase does not survive the field and is replaced by the M-state clock ordered phase for $h\neq 0$. For $M\geqslant 4$, however, the commensurability energy affects neither the transition temperature nor the nature of the transition.

We next take into consideration the effects of misfit and show in Fig. 9 the schematic phase diagram in the 3D space consisting of T, $U_\perp^{-1}$, and δ, with $U_\parallel$ and V_0 fixed. At $\delta=0$, the system belongs to the same university class as the

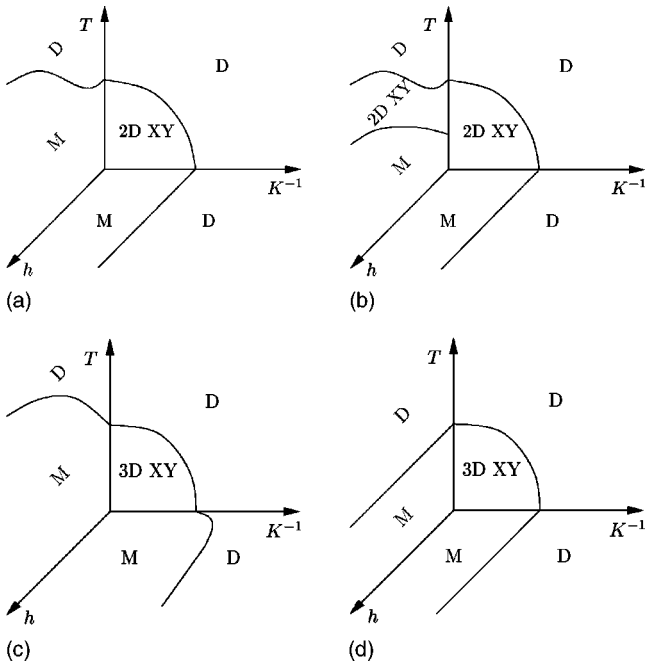

FIG. 8. Schematic phase diagram for the coupled commensurate CDW system in the (T,h,K^{-1}) space, depending on spatiotemporal fluctuations and commensurability: the homogeneous case (a) for $M=4$ and (b) for $M\geqslant 5$; the general case (c) for $M=2$ or 3 and (d) for $M\geqslant 4$. Plotted on each plane are boundaries between various phases, including the disordered phase (D), the M-state clock ordered phase (M), the algebraically ordered phase present in the 2D XY model (2D XY), and the 3D XY ordered phase (3D XY).

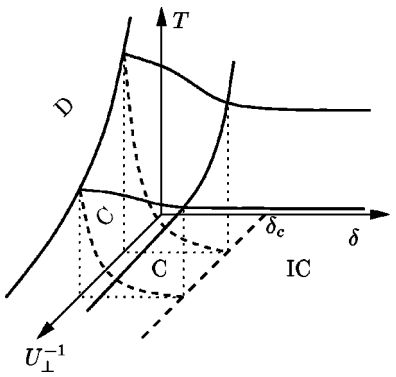

FIG. 9. Schematic phase diagram for the coupled CDW system in the $(T, U_\perp^{-1}, \delta)$ space, with the effects of the misfit taken into account. The surfaces depicted by thick solid lines and dashed lines separate the incommensurate CDW phase (IC) from the disordered phase (D) and from the commensurate CDW phase (C), respectively.

3D XY model under the symmetry-breaking field, for which the phase diagram is drawn on the T-$U_\perp^{-1}$ plane. On the other hand, at zero temperature, each CDW chain undergoes the CI transition with the critical misfit δ_c which is independent of the interchain coupling strength $U_\perp$. The order-disorder transition temperature T_D and the CI transition temperature T_{IC} obtained in Sec. V produce surfaces depicted by (thick) solid and dashed lines, respectively, in the $(T, U_\perp^{-1}, \delta)$ space. The phase diagram shows that for $\delta < \delta_c$ the system undergoes double transitions as the temperature is lowered: first, the order-disorder transition into the incommensurate CDW phase and then, the CI transition into the commensurate CDW phase. As revealed in Sec. V, a hysteresis takes place around the CI transition point, which manifest itself more clearly as the interchain coupling becomes stronger.

VII. CONCLUSION

To study phase transitions in coupled CDW systems, we have mapped the systems at zero temperature onto three- or four-dimensional XY models, depending on the spatiotemporal fluctuations, under symmetry-breaking fields which arise from the commensurability energy. Such techniques as ϵ expansion, mean-field theory, and the Monte Carlo method have then been applied to the obtained XY models. Revealed is a single second-order transition between the M-state clock order and disorder in both the three-dimensional and four-dimensional systems, except for the case $M=3$ in the four-dimensional system where the transition is of the first order. In particular, the commensurability with $M \geqslant 4$ has been observed not to change the properties of the transition including the critical temperature and exponents. Combining these zero-temperature $(T=0)$ results with the existing results in the absence of quantum (temporal) fluctuations $(K^{-1}=0)$ or of the symmetry-breaking field $(h=0)$, we have constructed boundaries separating various phases on the three planes ($T=0$, $K^{-1}=0$, and $h=0$) in the three-dimensional (T, K^{-1}, h) space. The boundaries near $T=0$ and near $K^{-1}=0$ can then be speculated through the use of finite-size scaling and semiclassical methods, respectively, thus giving a schematic phase diagram in the (T, K^{-1}, h) space.

We have also found via Monte Carlo simulations that the system with nonzero misfit undergoes a commensurate-incommensurate transition. The interchain interactions give rise to the correlations between neighboring CDW's in such a way that either the commensurate state or the incommensurate state is favored depending on the initial configuration: In the cooling process the CDW's remain incommensurate down to almost zero temperature while in the heating process a substantial amount of the commensurate CDW's survive thermal fluctuations.

At strong thermal or quantum fluctuations, i.e., at high T or small K, the system is in the disordered phase. No CDW is formed and the system is expected to be metallic. On the contrary, weak fluctuations (low T and large K) favor the M-state clock ordered phase, in which commensurate CDW's are developed as long as $\delta < \delta_c$. Accordingly, the interaction between the periodicity of the CDW and the underlying lattice periodicity drives the collective excitation to develop a gap, and the system becomes insulating. At moderate fluctuations or for large misfit $(\delta > \delta_c)$, on the other hand, incommensurate CDW's emerge. In this case the system may remain conducting through collective Fröhlich conduction, i.e., via sliding of the CDW's. Usually, the conductivity via such collective modes is lower than that via uncondensated electrons in the disordered phase (without CDW). In particular, the CDW may be pinned in the presence of impurities, sharply decreasing the conductivity. As the temperature is lowered, therefore, the system for weak quantum or thermal fluctuations becomes insulating via three possible routes, depending on the misfit and the interchain interaction: First, the commensurate CDW phase emerges directly from the high-temperature disordered phase; second, only the incommensurate CDW phase appears, reducing the conductivity; third, the incommensurate CDW phase appearing first is followed by the commensurate phase emerging via the commensurate-incommensurate transition.

Note that beginning with the Hamiltonian in Eq. (1), we have taken into account only phase fluctuations and disregarded amplitude fluctuations. The latter are in general irrelevant in the RG sense, expected not to affect nature of the phase transition. On the other hand, there still lacks conclusive understanding of the dynamic properties in various phases. It is thus desirable to consider the responses to external electromagnetic fields, and, for example, compute the conductivity, which can be obtained from the current or the average momentum in the presence of appropriate misfit. Detailed investigation of such dynamic responses is left for further study.

ACKNOWLEDGMENTS

We thank G.S. Jeon for helpful discussions and acknowledge the partial support from the Korea Science and Engineering Foundation through the SKOREA Program and from the Ministry of Education of Korea through the BK21 Program.

[1] S. Kagoshima, H. Nagasawa, and T. Sambongi, *One-Dimensional Conductors* (Springer-Verlag, Berlin, 1987).

[2] See, e. g., B. Grévin, Y. Berthier, G. Collin, and P. Mendels, Phys. Rev. Lett. **80**, 2405 (1998); H.W. Yeom, S. Takeda, E. Rotenberg, I. Matsuda, K. Horikoshi, J. Schaefer, C.M. Lee, S.D. Kevan, T. Ohta, T. Nagao, and S. Hasegawa, *ibid.* **82**, 4898 (1999); Y. Li, S.G. Lemay, J.H. Price, K. Cicak, K. O'Neill, K. Ringland, K.D. Finkelstein, J.D. Brock, and R.E. Thorne, *ibid.* **83**, 3514 (1999).

[3] S. Coutinho, P. Pitanga, and P. Lederer, Phys. Rev. B **23**, 4567 (1981).

[4] G. Grüner, *Density Waves in Solids* (Addison-Wesley, Reading, 1994).

[5] M. Wallin, E.S. Sørensen, S.M. Girvin, and A.P. Young, Phys. Rev. B **49**, 12 115 (1994); S.L. Sondhi, S.M. Girvin, J.P. Carini, and D. Shahar, Rev. Mod. Phys. **69**, 315 (1997).

[6] S. Doniach, Phys. Rev. B **24**, 5063 (1981); E. Simanek, *ibid.* **32**, 500 (1985); J.V. José, *ibid.* **29**, 2836 (1984); S. Kim and M.Y. Choi, *ibid.* **41**, 111 (1990). See also A. van Otterlo, K.-H. Wagenblast, R. Fazio, and G. Schön, *ibid.* **48**, 3316 (1993); B.J. Kim, J. Kim, S.Y. Park, and M.Y. Choi, *ibid.* **56**, 395 (1997).

[7] L. Onsager, Nuovo Cimento, Suppl. **6**, 279 (1949); R.P. Feynman, in *Progress in Low Temperature Physics*, edited by C. Gorter (North-Holland, Amsterdam, 1955), Vol. 1, p. 17.

[8] G.A. Williams, Phys. Rev. Lett. **59**, 1926 (1987); **61**, 1142 (1988).

[9] S.R. Shenoy, Phys. Rev. B **40**, 5056 (1989).

[10] G. Kohring, R.E. Shrock, and P. Wills, Phys. Rev. Lett. **57**, 1358 (1986); G. Kohring and R.E. Shrock, Nucl. Phys. B **288**, 397 (1987); H. Kleinert, *Gauge Fields in Condensed Matter* (World Scientific, Singapore, 1989), Vol. I, pp. 528–530; A.P. Gottlob and M. Hasenbusch, Physica A **201**, 593 (1993).

[11] J.M. Kosterlitz and D.J. Thouless, J. Phys. C **6**, 1181 (1973); J.M. Kosterlitz, *ibid.* **7**, 1046 (1974).

[12] J.V. José, L.P. Kadanoff, S. Kirkpatrick, and D.R. Nelson, Phys. Rev. B **16**, 1217 (1977).

[13] K.G. Wilson and M.E. Fisher, Phys. Rev. Lett. **28**, 240 (1972).

[14] J. Cardy, *Scaling and Renormalization in Statistical Physics* (Cambridge University Press, Cambridge, 1996), pp. 100–101.

[15] M.E.J. Newman and G.T. Barkema, *Monte Carlo Methods in Statistical Physics* (Oxford University Press, New York, 1999), pp. 219–228.

[16] D.J. Scalapino, R.L. Sugar, and W.D. Toussaint, Phys. Rev. B **34**, 6367 (1986).

[17] J. Rudnick, J. Phys. A **8**, 1125 (1975); D. Kim and R.J. Joseph, *ibid.* **8**, 891 (1975); T.W. Burkhardt, H.J.F. Knops, and M. den Nijs, *ibid.* **9**, L179 (1976); H.W.J. Blöte and R.H. Swendsen, Phys. Rev. Lett. **43**, 799 (1979); B. Nienhuis, E.K. Riedel, and M. Schick, Phys. Rev. B **23**, 6055 (1981); J. Lee and J.M. Kosterlitz, *ibid.* **43**, 1268 (1991); P.D. Scholten and L.J. Irakliotis, *ibid.* **48**, 1291 (1993).

[18] W.Y. Shih and D. Stroud, Phys. Rev. B **28**, 6575 (1983).

[19] See, e.g., M.Y. Choi, *Physics of Complex Low-Dimensional Systems* (Hanul, Seoul, 2000), pp. 49–57.

[20] P.S. Sahni, Phys. Rev. B **23**, 1325 (1981).

[21] B. Topič, U. Haeberlen, and R. Blinc, Phys. Rev. B **42**, 7790 (1990).

[22] R.A. Craven and S.F. Meyer, Phys. Rev. B **16**, 4583 (1977); R.M. Fleming, D.E. Moncton, D.B. McWhan, and F.J. DiSalvo, Phys. Rev. Lett. **45**, 576 (1981); J.-G. Yoon and S.-I. Kwun, Phys. Rev. B **35**, 8591 (1987).

[23] Here we disregard the possible existence of reentrance, which has been a source of controversy. See Ref. 6.